

---

# MAP: Low-compute Model Merging with Amortized Pareto Fronts via Quadratic Approximation

---

Lu Li<sup>1\*</sup>, Tianyu Zhang<sup>2,3\*</sup>, Zhiqi Bu<sup>4\*</sup>, Suyuchen Wang<sup>2</sup>, Huan He<sup>1</sup>, Jie Fu<sup>4</sup>,  
Yonghui Wu<sup>5</sup>, Jiang Bian<sup>5</sup>, Yong Chen<sup>1</sup>, Yoshua Bengio<sup>2</sup>

<sup>1</sup> University of Pennsylvania, <sup>2</sup> MILA <sup>3</sup> ServiceNow Research

<sup>4</sup> Amazon AI <sup>5</sup> HKUST <sup>6</sup> University of Florida

{luli1, huanhe, ychen}@upenn.edu

{tianyu.zhang, yoshua.bengio}@mila.quebec

zhiqibu@amazon.com, jiefu@ust.hk, {bianjiang, yonghui.wu}@ufl.edu

## Abstract

Model merging has emerged as an effective approach to combine multiple single-task models, fine-tuned from the same pre-trained model, into a multitask model. This process typically involves computing a weighted average of the model parameters without any additional training. Existing model-merging methods focus on enhancing average task accuracy. However, interference and conflicts between the objectives of different tasks can lead to trade-offs during model merging. In real-world applications, a set of solutions with various trade-offs can be more informative, helping practitioners make decisions based on diverse preferences. In this paper, we introduce a novel low-compute algorithm, Model Merging with Amortized Pareto Front (MAP). MAP identifies a Pareto set of scaling coefficients for merging multiple models to reflect the trade-offs. The core component of MAP is approximating the evaluation metrics of the various tasks using a quadratic approximation surrogate model derived from a pre-selected set of scaling coefficients, enabling amortized inference. Experimental results on vision and natural language processing tasks show that MAP can accurately identify the Pareto front. To further reduce the required computation of MAP, we propose (1) a Bayesian adaptive sampling algorithm and (2) a nested merging scheme with multiple stages.

## 1 Introduction

Large pre-trained foundation models have become available in many real-world applications [49, 44, 12]. This increasing availability has led to a popular practice of fine-tuning these pre-trained models to adapt to a wide range of downstream tasks. The practitioners can independently fine-tune the same pre-trained model, such as CLIP style models [38, 52, 56], large language models [5, 39, 45, 25] etc. and then release the fine-tuned models without releasing the training data. As the deployment of such fine-tuned models increases, the concept of model merging—combining models with identical architectures and initializations has emerged as a promising approach to combine their respective capabilities. This is useful, especially in scenarios where the training data for each task are private and cannot be shared, such as individual-level patient data in a hospital and behavior data in social media recommendation systems.

Existing methods for merging models typically involve calculating a weighted average of the parameters from multiple models to enhance performance uniformly across various tasks. However, this approach often overlooks the conflicts or interference among the diverse objectives of these

---

\*Equal contribution. This work does not relate to ZB’s position at Amazon.

tasks, which can lead to trade-offs in terms of model performance on various tasks. In real-world applications, it is often useful to obtain a set of Pareto optimal solutions rather than a single averaged model. Such solutions allow practitioners to choose among different trade-offs, depending on their specific needs. For example, hospitals specializing in certain areas might prefer a model that excels in specific tasks relevant to their specialty while maintaining adequate performance across a broader spectrum of diseases.

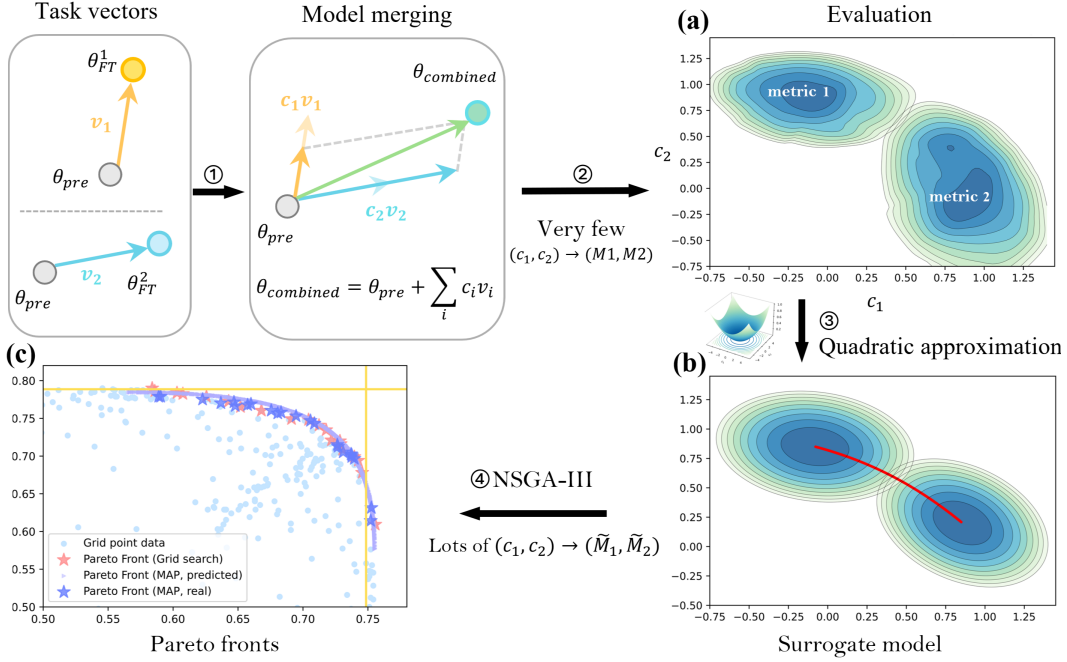


Figure 1: The overall process of MAP under 2 tasks. Step 1: select tasks and their corresponding task vectors. Step 2: sample a few scaling weights  $c$  to query the task metrics accordingly. Step 3: use a quadratic model to approximate the mapping of  $c \rightarrow metrics$  as a surrogate model. Step 4: use NSGA-III (or other multi-objective optimization algorithms) to find amortized Pareto fronts. Figure (a) shows the contour plots of the actual accuracy landscape for the ViT models [15] obtained from 100 scaling coefficients (sampled uniformly) evaluated on the SUN397[53] and Cars[27]. Figure (b) shows the contour plots of the fitted quadratic functions. Red lines represent the Pareto front in the decision variable  $(c_1, c_2)$  space. Figure (c) shows an example of the Pareto Front. Pareto front (Grid search) is regarded as the ground truth given the enough number of grid points. Pareto front (MAP, predicted) is the amortized Pareto front. Pareto front (MAP, real) is the Pareto front involving the same  $\{(c_1, c_2)\}$  but re-evaluated as to get the ground truth metrics as a comparison. The yellow lines are the evaluation performance of the fine-tuned single task models.

In this paper, we introduce a novel method that identifies the Pareto front without retraining the models to be merged. Our algorithm uses a quadratic approximation of the evaluation metric as the surrogate model, and further computes the Pareto front using existing evolutionary algorithms. Furthermore, we enhance it with a Bayesian adaptive sampling method and a nested merging scheme, which further brings down the computational cost. We validate our method across a diverse set of tasks, spanning from vision to natural language processing, and demonstrate its applicability to a variety of architectures, including ResNet [18], ViT [15], and large language models [5, 39, 45, 25].

**Contributions** The main contributions of this paper are:

- C1** Designing the quadratic surrogate models to approximate the evaluation metric functions, which amortize the computation of Pareto fronts;
- C2** Proposing a nested merging scheme to decrease computational complexity from exponential to quadratic;
- C3** Proposing the Bayesian adaptive sampling, which efficiently queries the computationally expensive evaluations according to the loss information.

**Related work** This paper is related to many existing works on multi-objective optimization, Pareto optimality, task arithmetic, federated/private learning, Bayesian methods, etc. We kindly refer the readers to Appendix A due to the page limit.

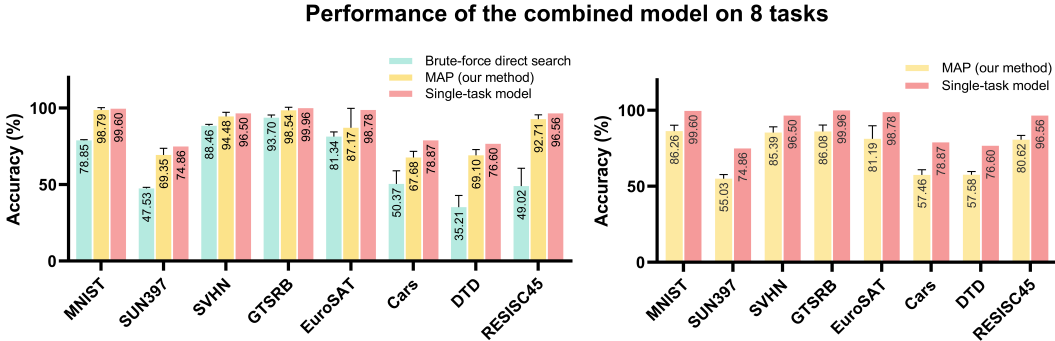


Figure 2: **(a)** Using the results of inference runs of merged ViT-B-32 models (CLIP checkpoints from [22]) obtained from 250 combinations of scaling coefficients, our method outperforms the direct search method in finding a set of diverse solutions for eight tasks based on the same computation expense. For both methods, we maximize a specific task while requiring all tasks to have an evaluation metric above a certain threshold (40%). The bar plot for each task shows the corresponding maximized accuracy. **(b)** We increase the requiring bounds to (65%) of the single-task model. With the same computational budget, the brute-force direct search method cannot find a feasible solution.

In Figure 2, we compare our method to the brute-force direct search. We emphasize our setting that evaluating models is computationally expensive, and therefore we can only query the evaluation pipeline a limited number of times. This setting makes the direct usage of evolutionary algorithms like NSGA-III infeasible (nevertheless, our usage of evolutionary algorithms on the surrogate models is feasible). In particular, evolutionary algorithms need to query the evaluation metrics so many times that exceeds our computational budget, because each query must evaluate all single-task models. To give more details, suppose we already have a set of solutions and know their evaluation metrics, and we use evolutionary algorithms to pick the Pareto solutions among them, then the set we find with the algorithms might not include all possible Pareto solutions. Instead, it will likely be just a part of what we would find if we have compared every possible pair of solutions directly against each other (known as brute force search). Since brute force search compares all possible solutions and finds all the Pareto optimums, it’s considered a complete method. Therefore, when evaluating the effectiveness of our algorithm, it is better to compare its results to those obtained from brute force search in the case of a limited set of already-known solutions. Our code is released here <https://github.com/luli-git/MAP.git>.

## 2 Background

### 2.1 Model merging

*Model merging* aims to find a way to combine multiple models with the same architecture  $\{\theta_{ft}^n\}_{n \in [N]}$  with their initialization  $\theta_{pre}$  in a way such that the merged model parameterized by  $\theta_m = \theta_{pre} + \sum_{n=1}^N c_n \theta_{ft}^n$  performs reasonably well on all  $N$  tasks [50].

A recent work by [22] introduced *task arithmetic* as a simple and effective way for performing model merging. The task vector for task  $n$  is defined as  $\mathbf{v}_n = \theta_{ft}^n - \theta_{pre}$ , which is the element-wise difference between the pre-trained parameters and the fine-tuned parameters for the task  $n$ . To perform the model merging with task vectors, we can compute  $\theta_{pre} + \sum_{n=1}^N c_n \mathbf{v}_n$ , where  $c_n$  is some scaling factors and has shown to be essential to the performance of the merged model [54, 55].

Denoting the metric of task  $n$  as  $M_n$ , most of the existing approaches for model merging aim to improve an equal weight average metric  $\frac{1}{N} \sum_{n=1}^N M_n$ . This target implies the user of the algorithm has equal preferences between tasks. However, in real-world applications, users might have biased preferences for the importance of tasks, necessitating trade-offs. In such cases, the goal of model merging is no longer the equal weight average metric. Instead, we need to answer a broader question:

Given any preferences over the set of tasks, what is the best way to merge the models?

## 2.2 Pareto fronts

**Pareto dominance** Let  $X$  be a set representing the solution space, where each element  $x \in X$  is a possible solution to the multi-objective optimization problem. Let there be  $n$  objectives. Define an evaluation function  $f_i : X \rightarrow \mathbb{R}$ , where  $i \in \{1, 2, \dots, n\}$ . Given two solutions  $x, y \in X$ , we define that  $x$  *Pareto dominates*  $y$ , denoted by  $x \succ_P y$ , if and only if:

$$\forall i \in \{1, 2, \dots, n\}, f_i(x) \leq f_i(y) \text{ and } \exists j \in \{1, 2, \dots, n\}, f_j(x) < f_j(y) \quad (1)$$

**Pareto optimal solutions** The Pareto front is the set of solutions in the solution space  $X$  that are not Pareto dominated by any other solutions in  $X$ .

$$\text{PF} = \{x \in X \mid \nexists y \in X \text{ s.t. } y \succ_P x\} \quad (2)$$

Pareto optimal solutions have been studied in multi-task (multi-objective) learning (MTL) [40, 30]. However, in most of the studies, approximating the Pareto front is computationally expensive and data inefficient. We introduce our method, MAP, a computationally efficient method to find the Pareto front for model merging.

## 3 Methods

### 3.1 Quadratic approximation of evaluation metric

Given the task vectors  $\{\mathbf{v}_n\}_{n \in [N]}$  and the initialization  $\boldsymbol{\theta}_{\text{pre}} \in \mathbb{R}^d$ , we denote the merged model parameters as  $\boldsymbol{\theta}_{\text{merge}}(\mathbf{c}) = \boldsymbol{\theta}_{\text{pre}} + \mathbf{V}\mathbf{c} = \boldsymbol{\theta}_{\text{pre}} + \sum_{n=1}^N c_n \mathbf{v}_n$ , where  $\mathbf{V} = \text{concat}(\mathbf{v}_1, \dots, \mathbf{v}_N) \in \mathbb{R}^{d \times N}$  is the task matrix and  $\mathbf{c} = \text{concat}(c_1, \dots, c_N) \in \mathbb{R}^N$  is the scaling coefficients for the task vectors.

We aim to optimize the evaluation metric for all tasks, denoted by  $M_n$ , via the multi-objective optimization (MOOP)<sup>2</sup>:

$$\min_{c_1, \dots, c_N} M_1(\mathbf{c}), \dots, M_N(\mathbf{c}) \quad (3)$$

This problem has  $N$  variables and  $N$  objectives, and we seek the Pareto optimal solutions.

To do so effectively and efficiently, we use the second-order Taylor expansion to approximate  $M_n$ :

$$\begin{aligned} M_n(\mathbf{c}) &\equiv M_n(\boldsymbol{\theta}_{\text{merge}}(\mathbf{c})) = M_n(\boldsymbol{\theta}_{\text{pre}}) + \nabla M_n(\boldsymbol{\theta}_{\text{pre}})^\top (\boldsymbol{\theta}_{\text{merge}}(\mathbf{c}) - \boldsymbol{\theta}_{\text{pre}}) \\ &\quad + \frac{1}{2} (\boldsymbol{\theta}_{\text{merge}}(\mathbf{c}) - \boldsymbol{\theta}_{\text{pre}})^\top \mathbf{H}_n(\boldsymbol{\theta}_{\text{pre}}) (\boldsymbol{\theta}_{\text{merge}}(\mathbf{c}) - \boldsymbol{\theta}_{\text{pre}}) + R_n(\boldsymbol{\theta}_{\text{merge}}(\mathbf{c}) - \boldsymbol{\theta}_{\text{pre}}) \\ &\approx M_n(\boldsymbol{\theta}_{\text{pre}}) + \nabla M_n(\boldsymbol{\theta}_{\text{pre}})^\top \mathbf{V}\mathbf{c} + \frac{1}{2} (\mathbf{V}\mathbf{c})^\top \mathbf{H}_t(\boldsymbol{\theta}_{\text{pre}}) \mathbf{V}\mathbf{c} \end{aligned}$$

where  $\mathbf{H}_n(\boldsymbol{\theta}_{\text{pre}}) = \nabla^2 M_n(\boldsymbol{\theta}_{\text{pre}}) \in \mathbb{R}^{d \times d}$  is the Hessian matrix and  $R_n(\boldsymbol{\theta}_{\text{merge}}(\mathbf{c}) - \boldsymbol{\theta}_{\text{pre}}) = R_n(\mathbf{V}\mathbf{c})$  is the third-order remainder, which is negligible when  $\|\mathbf{V}\mathbf{c}\|^3 = \|\boldsymbol{\theta}_{\text{merge}}(\mathbf{c}) - \boldsymbol{\theta}_{\text{pre}}\|^3$  is small. Note that the second-order Taylor expansion is widely used and provides a close approximation (see Figure 2 (a) and (b) and more discussion in Appendix A), as neural networks tend to converge close to their initialization, especially for fine-tuned models: it directly motivates Newton’s method, and supports the analysis of convergence [32, 6] and the scaling laws for large models [26, 20].

Leveraging this quadratic approximation, we can define surrogate models for each task  $n$ ,  $\tilde{M}_n(\mathbf{c}; \mathbf{A}_n, \mathbf{b}_n, e_n) \equiv e_n + \mathbf{b}_n^\top \mathbf{c} + \frac{1}{2} \mathbf{c}^\top \mathbf{A}_n \mathbf{c}$  and optimize the proxy problem of (3) via

$$\min_{c_1, \dots, c_T} \tilde{M}_1(\mathbf{c}), \dots, \tilde{M}_T(\mathbf{c}) \quad (4)$$

where

$$\mathbf{A}_n = \mathbf{V}^\top \mathbf{H}_n(\boldsymbol{\theta}_{\text{pre}}) \mathbf{V} \in \mathbb{R}^{T \times T}, \mathbf{b}_n = \mathbf{V}^\top \nabla M_n(\boldsymbol{\theta}_{\text{pre}}) \in \mathbb{R}^T, e_n = M_n(\boldsymbol{\theta}_{\text{pre}}) + R_n \quad (5)$$

<sup>2</sup>The evaluation metric  $M$  can be differentiable (e.g. the mean square loss or the cross-entropy/perplexity) or not necessarily (e.g. the classification accuracy, F1 score, BLEU or Rouge)

Importantly, (4) is parameterized in contrast to (3), with  $\frac{(N+1)(N+2)}{2}$  unknown coefficients in  $(e_n, \mathbf{b}_n, \mathbf{A}_n)$ <sup>3</sup>. Thus, we can further leverage existing methods to learn the coefficients by minimizing the empirical risk over multiple  $\mathbf{c}$ : for instance,

$$\mathbf{A}_n^*, \mathbf{b}_n^*, e_n^* = \arg \min_{\mathbf{A}_n, \mathbf{b}_n, e_n} \sum_{\mathbf{c} \in \Omega} |M_n(\boldsymbol{\theta}_{\text{merge}}(\mathbf{c})) - \tilde{M}_n(\mathbf{c}; \mathbf{A}_n, \mathbf{b}_n, e_n)|^2 \quad (6)$$

where  $\Omega = \{\mathbf{c}^{(1)}, \dots, \mathbf{c}^{(N_c)}\}$  is the set of  $\mathbf{c}$  and  $M_n(\boldsymbol{\theta}_{\text{merge}}(\mathbf{c}))$  is the corresponding evaluation metric.

If the evaluation metric spanning to the whole  $\mathbb{R}$ , we use the vanilla form of surrogate model:  $\tilde{M}_n(\mathbf{c}; \mathbf{A}_n, \mathbf{b}_n, e_n) \equiv e_n + \mathbf{b}_n^\top \mathbf{c} + \frac{1}{2} \mathbf{c}^\top \mathbf{A}_n \mathbf{c}$ . When the evaluation metric is restricted with  $\in [l, u]$ , such as accuracy  $\in [0, 1]$ , we would warp the quadratic part with a sigmoid function, i.e.  $\tilde{M}_n(\mathbf{c}; \mathbf{A}_n, \mathbf{b}_n, e_n) \equiv (u - l) \text{sigmoid}(e_n + \mathbf{b}_n^\top \mathbf{c} + \frac{1}{2} \mathbf{c}^\top \mathbf{A}_n \mathbf{c}) + l$ . Similarity, if the evaluation metric is restricted  $\in [l, +\infty)$ , a softplus function as wrapper would be beneficial  $\tilde{M}_n(\mathbf{c}; \mathbf{A}_n, \mathbf{b}_n, e_n) \equiv \text{softplus}(e_n + \mathbf{b}_n^\top \mathbf{c} + \frac{1}{2} \mathbf{c}^\top \mathbf{A}_n \mathbf{c}) + l$ . Please note that  $u, l$  mentioned here are specific to the feasible domain of the metric, not learnable parameters.

### 3.2 Model merging with amortized pareto fronts

In this section, we introduce our generalized algorithm for estimating the amortized Pareto fronts. As mentioned in Section 3.1, we approximate the evaluation metric  $M_n(\cdot)$  by a surrogate quadratic model  $\tilde{M}_n(\cdot)$ . We then utilize  $\tilde{M}_n(\cdot)$  to compute the amortized Pareto fronts. Please see the detailed experiments in Section 4 and the algorithm details in Algorithm 1.

---

#### Algorithm 1 MAP

---

- 1: Prepare models  $\{\boldsymbol{\theta}_{ft}^n\}$  and compute task vectors  $\{\mathbf{v}_n = \boldsymbol{\theta}_{ft}^n - \boldsymbol{\theta}_{\text{pre}}\}$ .
  - 2: **for**  $t \in [T]$  **do**
  - 3:   Sample  $N_c$  vectors of  $\mathbf{c} \in \mathbb{R}^N$ . Denote the set as  $\Omega$ .
  - 4:   **for**  $\mathbf{c} = [c_1, \dots, c_N] \in \Omega$  **do**
  - 5:     Compute  $\boldsymbol{\theta}_{\text{merge}}(\mathbf{c}) = \boldsymbol{\theta}_{\text{pre}} + c_1 \mathbf{v}_1 + \dots + c_N \mathbf{v}_N$ .
  - 6:     Derive the evaluation metric  $M_n(\boldsymbol{\theta}_{\text{merge}}(\mathbf{c}))$ .
  - 7:   Fit the quadratic approximation surrogate model  $\tilde{M}_n$  by learning  $\mathbf{A}_n^*, \mathbf{b}_n^*, e_n^*$  in (6).
  - 8: Apply MOOP algorithm (e.g. NSGA-III) to  $\{\tilde{M}_n\}$  and get the Pareto front
- 

### 3.3 Nested merging scheme

Empirically, we only need 30 pairs to get a good quality of Pareto front to merge 2 tasks, but due to the curse of dimensionality, we need exponentially more number of  $(\mathbf{c}, \{\tilde{M}_n(\boldsymbol{\theta}_{\text{merge}}(\mathbf{c}))\}_{n=1}^N)$  pairs to get a good quality of Pareto front in the case of 8 tasks. Theoretically, in the best case, the points to get a good quality of Pareto front for  $N$  is  $O(N^3)$ . In the worst case, when the curse of dimensionality dominates, it could be  $O(N \cdot 2^N)$ . Using the nested merging scheme, we reduce the computation complexity from  $O(N \cdot 2^N)$  to  $O(N \log_2^N)$ . Please refer to Table 5 for the detailed computational complexity comparison. Algorithm details are presented in Algorithm 2.

### 3.4 Bayesian adaptive sampling

We have discussed the strategy of bringing down the computation in the sense of big  $O$  notation. It is effective when the number of tasks involved in the Pareto fronts is high.

In the case of a relatively low number of tasks ( $N \leq 4$ ), we consider using the Bayesian adaptive sampling method inspired by Bayesian optimization.

In Algorithm 1, we only sample a single round of scaling weights  $\mathbf{c}$  and query the ground truth metric by evaluation through the  $M_n(\boldsymbol{\theta}_{\text{merge}}(\mathbf{c}))$ . In contrast, as for the Bayesian adaptive sampling, we sample the scaling weights  $\mathbf{c}$  in multiple rounds. In each round, the sampling strategy depends on the previous sampling  $\mathbf{c}$  and its evaluation metrics. The process begins with an initial uniform sampling of

---

<sup>3</sup> 1 coefficient for  $e_n$ ,  $N$  coefficients in  $\mathbf{b}_n$  and  $N(N+1)/2$  coefficients in  $\mathbf{A}_n$  due to its symmetry.

---

**Algorithm 2** Nested merging scheme
 

---

**Require:** A predetermined preference  $pref \in \mathbb{R}^N$  over the  $N$  tasks, the tuple of task, loss, task vector:  $G_n = (\text{task}_n, l_n, \theta_{ft}^n)$

- 1: Normalize  $pref$  to make sure the sum is 1
- 2: Initialize the set  $\tau = \{G_1, \dots, G_N\}$
- 3: **while**  $|\tau| > 1$  **do**
- 4: Find the pair of  $(G_i, G_j) \in \tau$  that are closest to each other in terms of  $(l_i, l_j)$
- 5: Implement Algorithm 1 to find the Pareto front  $\text{PF}_{i,j}$  between  $(\tilde{M}_i, \tilde{M}_j)$
- 6: Select the  $\mathbf{c}^* = (c_i^*, c_j^*) \in \mathbb{R}^2$  based on the Pareto front  $\text{PF}_{i,j}$
- 7: Merge the models by  $\theta_{\text{merge}}^{i,j} = \theta_{\text{pre}} + c_i(\theta_{ft}^i - \theta_{\text{pre}}) + c_j(\theta_{ft}^j - \theta_{\text{pre}})$
- 8: Calculate the weighted average loss on the two tasks  $l_{ij} = pref_i l_i + pref_j l_j$
- 9: Update  $\tau$  by replacing  $\{G_i, G_j\}$  with  $\{G_{ij}\}$ , where  $G_{ij} \equiv (\text{task}_{i,j}, l_{ij}, \theta_{\text{merge}}^{i,j})$
- 10: **return**  $\theta_{\text{merge}}^{1,2,\dots,N}$

---

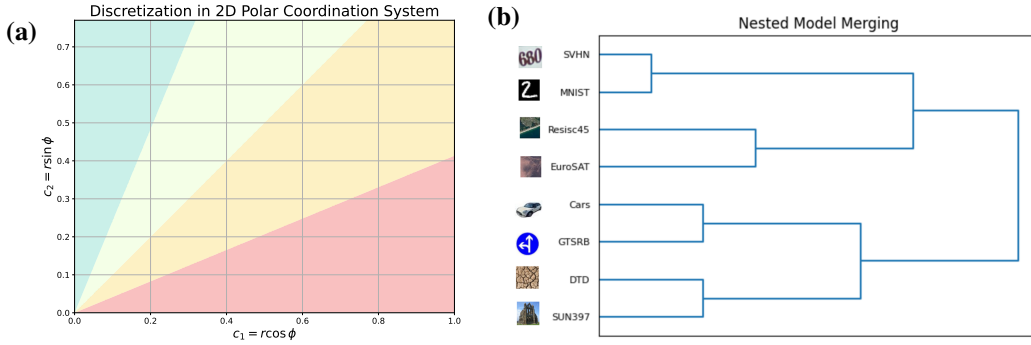


Figure 3: (a) Discretizing of two task scaling coefficients along the angular dimension in 2D polar coordinate system (please refer to Figure 9 for an example of 3D spherical discretization.); (b) An example of nested model merging for  $N = 6$  models (see more details in Appendix E);

scaling coefficients,  $\{(c_1, \dots, c_N)_{i=0}^{n_0}\}$ , from  $[0, 1]^T$ . For simplicity, we define  $\mathbf{c}_i$  as  $(c_1, \dots, c_N)_i$ . We evaluate the merged model  $\theta_m(\mathbf{c}_i)$  across tasks 1 to  $N$  and compute the corresponding  $L2$  loss. We then discretize the regions of  $\mathbf{c}$  into joint bins within a hyper-spherical coordinate system and discretize along the angular dimensions. Please refer to figure 9 as examples in 2-dimensional and 3-dimensional discretization. The posterior distribution is computed proportional to an acquisition function (e.g., upper confidence bound) of the approximation loss within specific bins.

We iteratively update each surrogate model for tasks  $\{t\}_{n=1}^N$ . See the algorithm 3 for a simplified version of the process. For more details, please refer to the Algorithm 4 in the appendix. After meeting the stopping criterion, we use the  $N$  surrogate models to generate a lot of  $(\mathbf{c}, \{\tilde{M}_n(\theta_m(\mathbf{c}))\}_{n=1}^N)$  pairs and apply MOOP algorithm (e.g. NSGA-III) to  $\{\tilde{M}_{n=1}^N\}$  to calculate the Pareto front.

## 4 Experiments

In this section, we present our empirical findings across a wide range of tasks including zero-shot classification (CLIP-based), and LLMs (Llama3-based).

Through our experiments, we aim to answer the following questions:

- Q1** How well do our surrogate quadratic functions approximate the true performance metric? How well do the amortized Pareto fronts approximate the ground truth Pareto front?
- Q2** For a smaller number of tasks ( $N < 4$ ), how many fewer queries would Bayesian adaptive sampling require compared to the traditional single-shot merging scheme?

---

**Algorithm 3** Bayesian Adaptive for Surrogate Model

---

**Require:** Number of iterations  $J$ , Buffer  $\mathcal{B}$ , Pretrained model  $\theta_{\text{pre}}$ , Task vectors  $\mathbf{V} = (\mathbf{v}_1, \dots, \mathbf{v}_n)$ , Evaluation function  $M_n(\cdot)$  for task  $n$ .

- 1: Initialize  $\mathcal{B}$  to an empty set.
- 2: **for** each iteration  $j = 0$  to  $J$  **do**
- 3:   Sample scaling coefficients  $\{\mathbf{c}_i\}_{i=1}^{n_j}$  based on updated distribution from previous results (uniformly sampled if  $j = 0$ ).
- 4:   **for** each scaling coefficient  $i = 1$  to  $n_j$  **do**
- 5:     Adjust the model with  $\theta_{\text{merge}}(\mathbf{c}_i) = \theta_{\text{pre}} + \mathbf{c}_i \cdot \mathbf{V}$ .
- 6:     Evaluate this model configuration  $m_{n,i} = M_n(\theta_{\text{merge}}(\mathbf{c}_i))$  and store  $(\mathbf{c}_i, m_{n,i})$  in  $\mathcal{B}$ .
- 7:   Update the surrogate model based on the  $(\mathbf{c}, \{\tilde{M}_n(\theta_{\text{merge}}(\mathbf{c}))\}_{n=1}^N)$  pairs in  $\mathcal{B}$ .
- 8:   Estimate acquisition function (UCB) for different model configurations.
- 9:   Adjust the sampling strategy for the next iteration based on these evaluation metrics.
- 10: **return**

---

**Q3** With identical preferences and computational budgets, how does the performance of the nested merging scheme compare to that of the traditional single-shot merging scheme?

#### 4.1 Experiment setup

Table 1: Experiment setup in terms of tasks and models

Task type	Metric	# of total tasks	Model type
Zero-shot Classification (normal)	Accuracy	8	ViT-B/32 (CLIP)
Zero-shot Classification (medical)	Accuracy	2	ViT-B/32 (CLIP)
Language Generation	Loss / Perplexity	4	Llama3-8B
Image Classification	Accuracy	3	ResNet-18

**Datasets and models** We study multi-task model merging on eight normal zero-shot image classification datasets following [22]: SUN397 [53], Cars [27], GTSRB [41], MNIST [29], EuroSAT [19], SHVN [34], DTD [10], RESISC45 [8]. We use the ViT-B/32 architecture in CLIP [38] as the pre-trained model for the experiments on vision tasks in the main text. We show the results of them in the main pages. For the rest of the experiments, due to the page limits, we show them in the appendix. The result of dataset and task we experiment on are as follows: a zero-shot medical chest x-ray image classification tasks to show our model merging scheme also works in a read world application domain [47]; 4 fine-tuned Llama3 models in different languages: French, Arabic, Chinese, and Japanese.<sup>4</sup>; 3 vision tasks on the ResNet18 architecture, CIFAR-10 [28], Flowers-102 [35], and GTSRB [41].

#### 4.2 Baseline and metrics

**Baseline** Our baseline method for obtaining Pareto fronts is the brute-force direct search. When the number of tasks is low ( $N < 4$ ), we can sample enough grid points of  $\mathbf{c}$  and query the corresponding evaluation metrics  $\{M_n(\theta_{\text{merge}}(\mathbf{c}))\}_{n=1}^N$ . We can then directly use the resulting evaluation metrics to find the Pareto front by direct comparisons of each task performance of the merged model by  $c_i \in \mathbf{c}$ . When the number of tasks is low, we can regard the resulting Pareto front as the ground truth Pareto front. However, when the number of tasks grows, the required number of  $(\mathbf{c}, \{M_n(\theta_{\text{merge}}(\mathbf{c}))\}_{n=1}^N)$  pairs grows exponentially, which is way larger than the points we evaluated. Thus, when the number of tasks is high ( $N \geq 4$ ), the results from the brute-force direct search can no longer be considered as ground truth.

**Win rate** We used the win rate to measure how often the Pareto front found by MAP outperforms the Pareto front found by the baseline in terms of multiple objectives. Let  $PF_{\text{MAP}}$  and  $PF_{\text{baseline}}$

---

<sup>4</sup>All the fine-tuned language Llama3 models can be found on huggingface. The IDs of the model are: French: jpacifico/French-Alpaca-Llama3-8B-Instruct-v1.0; Arabic: MohamedRashad/Arabic-Orpo-Llama-3-8B-Instruct; Chinese: shenzhi-wang/Llama3-8B-Chinese-Chat; Japanese: haqishen/Llama-3-8B-Japanese-Instruct.

represent the set of solutions in the Pareto fronts obtained from the MAP and the baseline methods, respectively. Each solution in these sets is a vector in  $\mathbb{R}^N$ , where  $N$  is the number of objectives or tasks. We sample  $K = \min(100, |PF_{\text{baseline}}|)$  points from each of the two Pareto fronts, denoted as  $\mathbf{c}_k^{\text{MAP}}$  and  $\mathbf{c}_k^{\text{baseline}}$ ,  $k = 1, \dots, K$ . Then, we compare  $M_n(\boldsymbol{\theta}_{\text{merge}}(\mathbf{c}_k^{\text{MAP}}))$  and  $M_n(\boldsymbol{\theta}_{\text{merge}}(\mathbf{c}_k^{\text{baseline}}))$  pairwise for  $k = 1, \dots, K$  and  $n = 1, \dots, N$ , resulting in  $K \times K \times N$  comparisons. The ratio of instances where  $M_n(\boldsymbol{\theta}_{\text{merge}}(\mathbf{c}_k^{\text{MAP}})) > M_n(\boldsymbol{\theta}_{\text{merge}}(\mathbf{c}_k^{\text{baseline}}))$  is computed as the win rate of our amortized Pareto front  $PF_{\text{MAP}}$ .

**Generational distance and inverted generational distance** We evaluated the quality of the Pareto front in capturing the shape of the ground truth Pareto front by measuring how much the predicted Pareto front converges to the ground truth Pareto front by calculating the generational distance (GD) [46] and how much the predicted Pareto front covers the ground truth Pareto front by calculating the inverted generational distance (IGD) [11]. GD and IGD are standard measures used in evolutionary multi-objective optimization to evaluate the solutions found by the evolutionary algorithms.

Given two solution sets  $PF_i = \{\tilde{M}_1^i(\boldsymbol{\theta}_{\text{merge}}(\mathbf{c})), \dots, \tilde{M}_N^i(\boldsymbol{\theta}_{\text{merge}}(\mathbf{c}))\}$ ,  $i = 1, 2$ , the GD and IGD metrics are defined as  $GD(PF_1) \equiv \frac{1}{K} \left( \sum_{i=1}^K d_i^p \right)^{1/p}$  and  $IGD(PF_1) \equiv \frac{1}{M} \left( \sum_{i=1}^M \tilde{d}_i^p \right)^{1/p}$  where  $d_i$  is the minimal Euclidean distance from  $\tilde{M}_1^1(\boldsymbol{\theta}_{\text{merge}}(\mathbf{c}))$  to  $PF_2$  and  $\tilde{d}_i$  is the minimal Euclidean distance from  $\tilde{M}_1^2(\boldsymbol{\theta}_{\text{merge}}(\mathbf{c}))$  to  $PF_1$ .

### 4.3 Win rate of MAP over the direct search method

Our findings indicate that for a small number of tasks ( $N < 4$ ), we achieve similar performance to the ground truth Pareto front with only 30 to 50 evaluation queries of  $(\mathbf{c}, M_n(\boldsymbol{\theta}_{\text{merge}}(\mathbf{c})))_{n=1}^N$  pairs. However, in scenarios with a higher number of tasks ( $N \geq 4$ ), MAP significantly outperforms the brute-force (non-ground truth) Pareto solutions. This is because, as detailed in Section 4.2, the number of required  $(\mathbf{c}, M_n(\boldsymbol{\theta}_{\text{merge}}(\mathbf{c})))_{n=1}^N$  pairs increases exponentially with the number of tasks. This exponential growth far exceeds the number of pairs that can be realistically evaluated.

For instance, when  $N = 3$  and we have 50  $(\mathbf{c}, M_n(\boldsymbol{\theta}_{\text{merge}}(\mathbf{c})))_{n=1}^N$  pairs, the approximate number of points on the grid line is around  $\sqrt[3]{50} \approx 6.69$ . However, when  $N$  increases to 8, achieving 5 points on each grid line would require  $5^8 = 390,625$  total points to evaluate, which is significantly more than the 1,000 points we realistically evaluated.

Table 2: Win rate of the amortized Pareto front and the Pareto front by brute-force direct search. The number of points is the number of points each algorithm used to find the Pareto front. Note that the number of evaluations by each method is the number of points multiplied by the number of tasks. The number of points per dimension is the number of points raised to the power of  $\frac{1}{N}$ , which measures the sparsity of points the direct search method uses per dimension to approximate the Pareto front. Subscripts denote standard deviations over 3 runs.

# of tasks	# of pts direct search	# of pts per dim	# of pts (MAP)	Win rate (MAP)	$R^2$ (MAP)
2	200	14.14	30	49.81% ( $\pm 0.30$ )	0.953 ( $\pm 0.018$ )
3	300	6.69	50	46.90% ( $\pm 0.71$ )	0.980 ( $\pm 0.003$ )
4	300	4.16	60	50.67% ( $\pm 2.44$ )	0.984 ( $\pm 0.004$ )
5	500	3.47	85	53.00% ( $\pm 1.88$ )	0.941 ( $\pm 0.019$ )
6	500	2.82	100	60.71% ( $\pm 1.34$ )	0.941 ( $\pm 0.030$ )
7	1000	2.68	140	63.42% ( $\pm 1.91$ )	0.891 ( $\pm 0.024$ )
8	1000	2.37	250	65.58% ( $\pm 0.94$ )	0.868 ( $\pm 0.028$ )

### 4.4 Performance of the quadratic approximation

We further validated the quadratic approximation of the surrogate models and the true performance by measuring the out-of-sample  $R^2$ . Figure 4 shows the relationship between the average  $R^2$  across all tasks and the number of total points used to fit the quadratic function. As we can see from Figure 4 (a), the average  $R^2$  values are close to 1 when the dimension of the decision space is low ( $N < 4$ )



when using around 30 points. However, as the dimension of the decision space increases ( $N \geq 4$ ), the average  $R^2$  depends more heavily on the number of points (Figure 4 (b)).

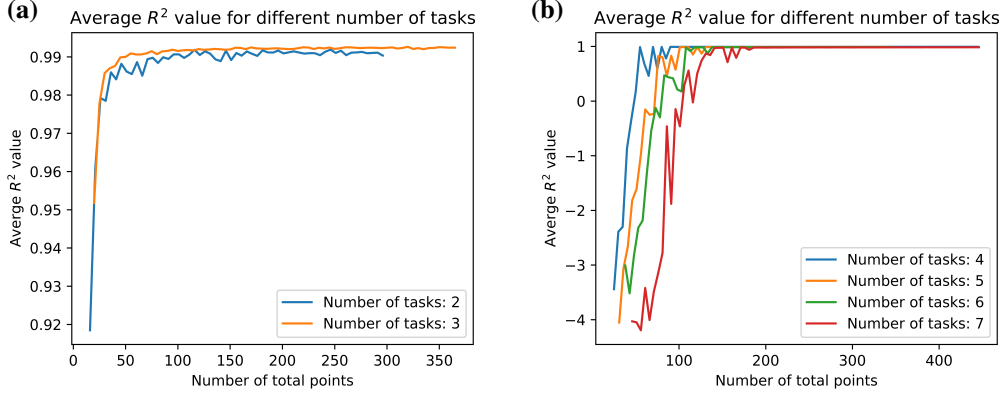


Figure 4: (a) An example of uncertainty in 2D polar coordinate system. The more uncertain within a bin, the more  $(\mathbf{c}, \{M_n(\theta_{\text{merge}}(\mathbf{c}))\}_{n=1}^N)$  pairs information we should collect in the next round. (b) An illustration of discretization of a 3D spherical coordinate system. When the dimension is higher, the discretization would be in a hyper-spherical coordinate system along with the angular dimensions.

#### 4.5 Bayesian adaptive sampling algorithm

We further improve the efficiency of MAP by proposing an adaptive Bayesian sampling algorithm. This Bayesian approach samples the points from regions with the highest level of uncertainty, where uncertainty is quantified with the Upper confidence bound (UCB).

Below, we define points (pts) as scaling coefficients and evaluation metrics of the corresponding merged models.

All of these experiments are initialized with 6 pairs of  $\mathbf{c}, \{M_n\}_{n=1}^N$  (iter 0). In every following iteration, we sample more points following the Bayesian adaptive sampling algorithm. We compare the Bayesian adaptive sampling beginning with 6 points and adding 3 additional points (6+3 pts) with running Algorithm 1 with 9 points in a row. We also compare the Bayesian adaptive sampling beginning with 6 points and adding 3 additional points 2 times (6+2 $\times$ 3 pts) with running Algorithm 1 with 12 points in a row.

We show that, utilizing the same number of points, Bayesian adaptive sampling performs better than the run-in-a-row scheme in Algorithm 1. The metrics in Figure 7 are average numbers over 7 experiments in different datasets. Please refer to Table 7 for detailed results in every experiment.

Table 3: Results obtained using Bayesian adaptive sampling using 3 iterations. The initial number of points is 6, and we sample an additional 3 points using the Bayesian adaptive sampling method. The “init  $n$ ” shows the metrics when we use  $n$  points to calculate the amortized Pareto front in a single row. Subscripts denote standard deviations over 6 runs.

	Iter 0 (6 pts)	Iter 1 (6+3 pts)	Init 9	Iter 2 (6+3 $\times$ 2 pts)	Init 12
GD ( $\downarrow$ )	0.234 <sub>0.154</sub>	<b>0.11</b> <sub>0.085</sub>	0.118 <sub>0.106</sub>	<b>0.079</b> <sub>0.062</sub>	0.091 <sub>0.082</sub>
IGD ( $\downarrow$ )	0.124 <sub>0.118</sub>	<b>0.047</b> <sub>0.082</sub>	0.067 <sub>0.09</sub>	0.038 <sub>0.053</sub>	<b>0.034</b> <sub>0.037</sub>
GD+IGD ( $\downarrow$ )	0.357 <sub>0.211</sub>	<b>0.158</b> <sub>0.137</sub>	0.185 <sub>0.165</sub>	<b>0.118</b> <sub>0.08</sub>	0.125 <sub>0.101</sub>
$R_0^2$ ( $\uparrow$ )	-2.237 <sub>3.792</sub>	<b>-0.103</b> <sub>2.218</sub>	-0.194 <sub>1.675</sub>	<b>0.459</b> <sub>0.784</sub>	0.44 <sub>0.902</sub>
$R_1^2$ ( $\uparrow$ )	-1.186 <sub>2.291</sub>	<b>0.342</b> <sub>0.959</sub>	0.165 <sub>1.33</sub>	<b>0.428</b> <sub>0.844</sub>	0.409 <sub>0.27</sub>

#### 4.6 Reduction of the number of models merged simultaneously

We performed nested model merging on four tasks and compared its performance with merging four tasks directly. When merging two models, we require that all models should achieve 70% of the

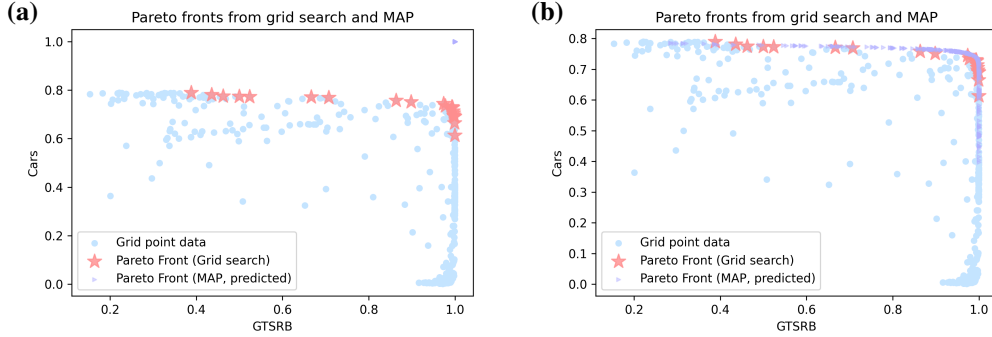


Figure 5: (a) This plot shows a failure case of amortized Pareto front when we only have 6 initial randomly sampled pairs of  $(c, \{M_i(\theta_m(c))\}_{i=1}^N)$  (b) After one iteration of Bayesian adaptive sampling for 3 more pairs (9 in total), our amortized Pareto front much better than the previous one.

single-task fine-tuned model, while maximizing the performance on the first task. We note that even though we require that all models should achieve 70% of the single-task fine-tuned model, the nested merging method can only achieve 60% of the single-task fine-tuned models during the final combine. Therefore, in Table 4, we report the results when we require achieving at least 60% of each task’s single-task fine-tuned model. From the Table 4, we can conclude that even if the nested merging scheme needs way fewer queries of evaluation metric calculations compared to directly merging 4 models, it is still capable of recovering more than 80 percent performances of directly merging 4 models and sometimes even higher than the directly merging scheme. The direct merging approach uses 80 evaluation queries, while the nested merging uses 20 evaluation queries in each round of merging.

Table 4: Accuracy on four tasks when using nested merging vs direct merging. We first merge models 1 and 2, and models 3 and 4 in parallel, using the preference that requires all tasks to have a normalized performance of at least 70% while optimizing the performance on tasks (1 and 3). We then compute the Pareto front for the two combined models. The table shows the highest accuracies on each task, while requiring all tasks to achieve a normalized performance of 65%. Subscripts denote standard deviations over 10 runs.

	SUN397 (1)	DTD (2)	GTSRB (3)	Cars (4)
Nested merging	<b>73.24</b> <sub>1.03</sub>	50.69 <sub>1.67</sub>	96.26 <sub>0.31</sub>	56.20 <sub>3.46</sub>
Directly merge 4 models	68.36 <sub>2.63</sub>	<b>61.70</b> <sub>6.78</sub>	<b>98.97</b> <sub>0.41</sub>	<b>68.24</b> <sub>3.38</sub>
Performance recovering	107%	82.2%	97.3%	82.4%

## 5 Conclusion and Limitations

Our method (MAP) can serve as an out-of-box plug-in that can easily combine with other model merging methods, including but not limited to linear merging model [50] and tasks arithmetic [22]. From the Section 3 and Section 4, we have shown that our method Algorithm 1, Algorithm 2, Algorithm 3 can efficiently bring down the computational cost from  $O(N \cdot 2^N)$  to  $O(N \cdot \log_2 N)$ , which are even less costly in the parameter-efficient training (e.g. LoRA). However, we would like to point out some limitations of our method. First, during the design of the Algorithm 1, we do not deal with the situation of the non-convex Pareto front. In the case of 2 tasks, most likely the Pareto fronts with proper trade-offs would have a convex Pareto front, but if we deal with more tasks, it is very likely that the ground truth Pareto fronts are non-convex and we will end up with approximating a convex hull with Algorithm 1. A quick but naive fix would be to implement Algorithm 2 in this case so that the Pareto fronts between 2 tasks would be more likely to be convex. Second, we don’t have a detector algorithm to detect if 2 tasks have proper trade-offs. Trying to approximate a Pareto front with only one Pareto solution inside will result in very unstable and bad-perform results. The practitioners should be informed in this case.

## References

- [1] Zeyuan Allen-Zhu, Yuanzhi Li, and Zhao Song. A convergence theory for deep learning via over-parameterization. In *International conference on machine learning*, pages 242–252. PMLR, 2019.
- [2] Anne Auger, Johannes Bader, Dimo Brockhoff, and Eckart Zitzler. Theory of the hypervolume indicator: optimal  $\mu$ -distributions and the choice of the reference point. In *Proceedings of the tenth ACM SIGEVO workshop on Foundations of genetic algorithms*, pages 87–102, 2009.
- [3] Oscar Brito Augusto, Fouad Bennis, Stephane Caro, et al. Multiobjective optimization involving quadratic functions. *Journal of optimization*, 2014, 2014.
- [4] Nicola Beume, Boris Naujoks, and Michael Emmerich. Sms-emoa: Multiobjective selection based on dominated hypervolume. *European Journal of Operational Research*, 181(3):1653–1669, 2007.
- [5] Tom Brown, Benjamin Mann, Nick Ryder, Melanie Subbiah, Jared D Kaplan, Prafulla Dhariwal, Arvind Neelakantan, Pranav Shyam, Girish Sastry, Amanda Askell, et al. Language models are few-shot learners. *Advances in neural information processing systems*, 33:1877–1901, 2020.
- [6] Zhiqi Bu, Xinwei Zhang, Mingyi Hong, Sheng Zha, and George Karypis. Pre-training differentially private models with limited public data. *arXiv preprint arXiv:2402.18752*, 2024.
- [7] Sébastien Bubeck et al. Convex optimization: Algorithms and complexity. *Foundations and Trends® in Machine Learning*, 8(3-4):231–357, 2015.
- [8] Gong Cheng, Junwei Han, and Xiaoqiang Lu. Remote sensing image scene classification: Benchmark and state of the art. *Proceedings of the IEEE*, 105(10):1865–1883, 2017.
- [9] Lenaïc Chizat, Edouard Oyallon, and Francis Bach. On lazy training in differentiable programming. *Advances in neural information processing systems*, 32, 2019.
- [10] Mircea Cimpoi, Subhansu Maji, Iasonas Kokkinos, Sammy Mohamed, and Andrea Vedaldi. Describing textures in the wild. In *Proceedings of the IEEE conference on computer vision and pattern recognition*, pages 3606–3613, 2014.
- [11] Carlos A Coello Coello and Nareli Cruz Cortés. Solving multiobjective optimization problems using an artificial immune system. *Genetic programming and evolvable machines*, 6:163–190, 2005.
- [12] Haotian Cui, Chloe Wang, Hassaan Maan, Kuan Pang, Fengning Luo, Nan Duan, and Bo Wang. scgpt: toward building a foundation model for single-cell multi-omics using generative ai. *Nature Methods*, pages 1–11, 2024.
- [13] Kalyanmoy Deb and Himanshu Jain. An evolutionary many-objective optimization algorithm using reference-point-based nondominated sorting approach, part i: solving problems with box constraints. *IEEE transactions on evolutionary computation*, 18(4):577–601, 2013.
- [14] Kalyanmoy Deb, Manikant Mohan, and Shikhar Mishra. Towards a quick computation of well-spread pareto-optimal solutions. In *Evolutionary Multi-Criterion Optimization: Second International Conference, EMO 2003, Faro, Portugal, April 8–11, 2003. Proceedings 2*, pages 222–236. Springer, 2003.
- [15] Alexey Dosovitskiy, Lucas Beyer, Alexander Kolesnikov, Dirk Weissenborn, Xiaohua Zhai, Thomas Unterthiner, Mostafa Dehghani, Matthias Minderer, Georg Heigold, Sylvain Gelly, et al. An image is worth 16x16 words: Transformers for image recognition at scale. *arXiv preprint arXiv:2010.11929*, 2020.
- [16] Simon Du, Jason Lee, Haochuan Li, Liwei Wang, and Xiyu Zhai. Gradient descent finds global minima of deep neural networks. In *International conference on machine learning*, pages 1675–1685. PMLR, 2019.
- [17] Saeed Ghadimi and Guanghui Lan. Stochastic first-and zeroth-order methods for nonconvex stochastic programming. *SIAM journal on optimization*, 23(4):2341–2368, 2013.
- [18] Kaiming He, Xiangyu Zhang, Shaoqing Ren, and Jian Sun. Deep residual learning for image recognition. In *Proceedings of the IEEE conference on computer vision and pattern recognition*, pages 770–778, 2016.
- [19] Patrick Helber, Benjamin Bischke, Andreas Dengel, and Damian Borth. Eurosat: A novel dataset and deep learning benchmark for land use and land cover classification. *IEEE Journal of Selected Topics in Applied Earth Observations and Remote Sensing*, 12(7):2217–2226, 2019.
- [20] Jordan Hoffmann, Sebastian Borgeaud, Arthur Mensch, Elena Buchatskaya, Trevor Cai, Eliza Rutherford, Diego de Las Casas, Lisa Anne Hendricks, Johannes Welbl, Aidan Clark, et al. Training compute-optimal large language models. *arXiv preprint arXiv:2203.15556*, 2022.
- [21] Evan J Hughes. Evolutionary many-objective optimisation: many once or one many? In *2005 IEEE congress on evolutionary computation*, volume 1, pages 222–227. IEEE, 2005.
- [22] Gabriel Ilharco, Marco Tulio Ribeiro, Mitchell Wortsman, Suchin Gururangan, Ludwig Schmidt, Hannaneh Hajishirzi, and Ali Farhadi. Editing models with task arithmetic. *arXiv preprint arXiv:2212.04089*, 2022.

- [23] Moksh Jain, Emmanuel Bengio, Alex Hernández-García, Jarrid Rector-Brooks, Bonaventure F. P. Dossou, Chanakya Ajit Ekbote, Jie Fu, Tianyu Zhang, Michael Kilgour, Dinghuai Zhang, Lena Simine, Payel Das, and Yoshua Bengio. Biological sequence design with gflownets. In Kamalika Chaudhuri, Stefanie Jegelka, Le Song, Csaba Szepesvári, Gang Niu, and Sivan Sabato, editors, *International Conference on Machine Learning, ICML 2022, 17-23 July 2022, Baltimore, Maryland, USA*, volume 162 of *Proceedings of Machine Learning Research*, pages 9786–9801. PMLR, 2022.
- [24] Moksh Jain, S. Rapparthi, Alex Hernández-García, Jarrid Rector-Brooks, Y. Bengio, Santiago Miret, and Emmanuel Bengio. Multi-objective gflownets. *International Conference on Machine Learning*, 2022.
- [25] Albert Q. Jiang, Alexandre Sablayrolles, Antoine Roux, Arthur Mensch, Blanche Savary, Chris Bamford, Devendra Singh Chaplot, Diego de las Casas, Emma Bou Hanna, Florian Bressand, Gianna Lengyel, Guillaume Bour, Guillaume Lample, Léo Renard Lavaud, Lucile Saulnier, Marie-Anne Lachaux, Pierre Stock, Sandeep Subramanian, Sophia Yang, Szymon Antoniak, Teven Le Scao, Théophile Gervet, Thibaut Lavril, Thomas Wang, Timothée Lacroix, and William El Sayed. Mixtral of experts. *arXiv preprint arXiv:2401.04088*, 2024.
- [26] Jared Kaplan, Sam McCandlish, Tom Henighan, Tom B Brown, Benjamin Chess, Rewon Child, Scott Gray, Alec Radford, Jeffrey Wu, and Dario Amodei. Scaling laws for neural language models. *arXiv preprint arXiv:2001.08361*, 2020.
- [27] Jonathan Krause, Michael Stark, Jia Deng, and Li Fei-Fei. 3d object representations for fine-grained categorization. In *Proceedings of the IEEE international conference on computer vision workshops*, pages 554–561, 2013.
- [28] Alex Krizhevsky, Geoffrey Hinton, et al. Learning multiple layers of features from tiny images. 2009.
- [29] Yann LeCun. The mnist database of handwritten digits. <http://yann.lecun.com/exdb/mnist/>, 1998.
- [30] Xi Lin, Hui-Ling Zhen, Zhenhua Li, Qing-Fu Zhang, and Sam Kwong. Pareto multi-task learning. *Advances in neural information processing systems*, 32, 2019.
- [31] Michael S Matena and Colin A Raffel. Merging models with fisher-weighted averaging. *Advances in Neural Information Processing Systems*, 35:17703–17716, 2022.
- [32] Sam McCandlish, Jared Kaplan, Dario Amodei, and OpenAI Dota Team. An empirical model of large-batch training. *arXiv preprint arXiv:1812.06162*, 2018.
- [33] Henry B. Moss, David S. Leslie, Daniel Beck, Javier Gonzalez, and Paul Rayson. Boss: Bayesian optimization over string spaces. In *Advances in Neural Information Processing Systems*, 2020.
- [34] Yuval Netzer, Tao Wang, Adam Coates, Alessandro Bissacco, Baolin Wu, Andrew Y Ng, et al. Reading digits in natural images with unsupervised feature learning. In *NIPS workshop on deep learning and unsupervised feature learning*, volume 2011, page 7. Granada, Spain, 2011.
- [35] Maria-Elena Nilsback and Andrew Zisserman. Automated flower classification over a large number of classes. In *2008 Sixth Indian conference on computer vision, graphics & image processing*, pages 722–729. IEEE, 2008.
- [36] National Institutes of Health et al. Nih clinical center provides one of the largest publicly available chest x-ray datasets to scientific community, 2017.
- [37] E. O. Pyzer-Knapp. Bayesian optimization for accelerated drug discovery. *IBM Journal of Research and Development*, 62(6):2:1–2:7, 2018.
- [38] Alec Radford, Jong Wook Kim, Chris Hallacy, Aditya Ramesh, Gabriel Goh, Sandhini Agarwal, Girish Sastry, Amanda Askell, Pamela Mishkin, Jack Clark, et al. Learning transferable visual models from natural language supervision. In *International conference on machine learning*, pages 8748–8763. PMLR, 2021.
- [39] Baptiste Rozière, Jonas Gehring, Fabian Gloeckle, Sten Sootla, Itai Gat, Xiaoqing Ellen Tan, Yossi Adi, Jingyu Liu, Romain Sauvestre, Tal Remez, Jérémy Rapin, Artyom Kozhevnikov, Ivan Evtimov, Joanna Bitton, Manish Bhatt, Cristian Canton Ferrer, Aaron Grattafori, Wenhan Xiong, Alexandre Défossez, Jade Copet, Faisal Azhar, Hugo Touvron, Louis Martin, Nicolas Usunier, Thomas Scialom, and Gabriel Synnaeve. Code llama: Open foundation models for code. *arXiv preprint arXiv:2308.12950*, 2023.
- [40] Ozan Sener and Vladlen Koltun. Multi-task learning as multi-objective optimization. In S. Bengio, H. Wallach, H. Larochelle, K. Grauman, N. Cesa-Bianchi, and R. Garnett, editors, *Advances in Neural Information Processing Systems*, volume 31. Curran Associates, Inc., 2018.
- [41] Johannes Stalldkamp, Marc Schlipf, Jan Salmen, and Christian Igel. The german traffic sign recognition benchmark: a multi-class classification competition. In *The 2011 international joint conference on neural networks*, pages 1453–1460. IEEE, 2011.
- [42] Hui Su, Zhi Tian, Xiaoyu Shen, and Xunliang Cai. Unraveling the mystery of scaling laws: Part i. *arXiv preprint arXiv:2403.06563*, 2024.

- [43] Kei Terayama, Masato Sumita, Ryo Tamura, and Koji Tsuda. Black-box optimization for automated discovery. *Accounts of Chemical Research*, XXXX, 02 2021.
- [44] Arun James Thirunavukarasu, Darren Shu Jeng Ting, Kabilan Elangovan, Laura Gutierrez, Ting Fang Tan, and Daniel Shu Wei Ting. Large language models in medicine. *Nature medicine*, 29(8):1930–1940, 2023.
- [45] Hugo Touvron, Louis Martin, Kevin Stone, Peter Albert, Amjad Almahairi, Yasmine Babaei, Nikolay Bashlykov, Soumya Batra, Prajjwal Bhargava, Shruti Bhosale, Dan Bikel, Lukas Blecher, Cristian Canton Ferrer, Moya Chen, Guillem Cucurull, David Esiobu, Jude Fernandes, Jeremy Fu, Wenyin Fu, Brian Fuller, Cynthia Gao, Vedanuj Goswami, Naman Goyal, Anthony Hartshorn, Saghar Hosseini, Rui Hou, Hakan Inan, Marcin Kardas, Viktor Kerkez, Madian Khabsa, Isabel Kloumann, Artem Korenev, Punit Singh Koura, Marie-Anne Lachaux, Thibaut Lavril, Jenya Lee, Diana Liskovich, Yinghai Lu, Yuning Mao, Xavier Martinet, Todor Mihaylov, Pushkar Mishra, Igor Molybog, Yixin Nie, Andrew Poulton, Jeremy Reizenstein, Rashi Rungta, Kalyan Saladi, Alan Schelten, Ruan Silva, Eric Michael Smith, Ranjan Subramanian, Xiaoqing Ellen Tan, Binh Tang, Ross Taylor, Adina Williams, Jian Xiang Kuan, Puxin Xu, Zheng Yan, Iliyan Zarov, Yuchen Zhang, Angela Fan, Melanie Kambadur, Sharan Narang, Aurelien Rodriguez, Robert Stojnic, Sergey Edunov, and Thomas Scialom. Llama 2: Open foundation and fine-tuned chat models. *arXiv preprint arXiv: 2307.09288*, 2023.
- [46] David Allen Van Veldhuizen. *Multiobjective evolutionary algorithms: classifications, analyses, and new innovations*. Air Force Institute of Technology, 1999.
- [47] Xiaosong Wang, Yifan Peng, Le Lu, Zhiyong Lu, Mohammadhadi Bagheri, and Ronald M Summers. Chestx-ray8: Hospital-scale chest x-ray database and benchmarks on weakly-supervised classification and localization of common thorax diseases. In *Proceedings of the IEEE conference on computer vision and pattern recognition*, 2017.
- [48] James T. Wilson, Riccardo Moriconi, Frank Hutter, and Marc Peter Deisenroth. The reparameterization trick for acquisition functions, 2017.
- [49] Michael Wornow, Rahul Thapa, Ethan Steinberg, Jason Fries, and Nigam Shah. Ehrshot: An ehr benchmark for few-shot evaluation of foundation models. 2023.
- [50] Mitchell Wortsman, Gabriel Ilharco, S. Gadre, R. Roelofs, Raphael Gontijo-Lopes, Ari S. Morcos, Hongseok Namkoong, Ali Farhadi, Y. Carmon, Simon Kornblith, and Ludwig Schmidt. Model soups: averaging weights of multiple fine-tuned models improves accuracy without increasing inference time. *International Conference on Machine Learning*, 2022.
- [51] Mitchell Wortsman, Gabriel Ilharco, Jong Wook Kim, Mike Li, Simon Kornblith, Rebecca Roelofs, Raphael Gontijo Lopes, Hannaneh Hajishirzi, Ali Farhadi, Hongseok Namkoong, et al. Robust fine-tuning of zero-shot models. In *Proceedings of the IEEE/CVF conference on computer vision and pattern recognition*, pages 7959–7971, 2022.
- [52] Yusong Wu, Ke Chen, Tianyu Zhang, Yuchen Hui, Taylor Berg-Kirkpatrick, and Shlomo Dubnov. Large-scale contrastive language-audio pretraining with feature fusion and keyword-to-caption augmentation. In *IEEE International Conference on Acoustics, Speech and Signal Processing ICASSP 2023, Rhodes Island, Greece, June 4-10, 2023*, pages 1–5. IEEE, 2023.
- [53] Jianxiong Xiao, Krista A Ehinger, James Hays, Antonio Torralba, and Aude Oliva. Sun database: Exploring a large collection of scene categories. *International Journal of Computer Vision*, 119:3–22, 2016.
- [54] Prateek Yadav, Derek Tam, Leshem Choshen, Colin A Raffel, and Mohit Bansal. Ties-merging: Resolving interference when merging models. *Advances in Neural Information Processing Systems*, 36, 2024.
- [55] Enneng Yang, Zhenyi Wang, Li Shen, Shiwei Liu, Guibing Guo, Xingwei Wang, and Dacheng Tao. Adamerging: Adaptive model merging for multi-task learning. *arXiv preprint arXiv:2310.02575*, 2023.
- [56] Xiaohua Zhai, Basil Mustafa, Alexander Kolesnikov, and Lucas Beyer. Sigmoid loss for language image pre-training. *IEEE International Conference on Computer Vision*, 2023.

## A Related Work

**Multi-objective optimization** Multi-objective optimization (MOOP) aims at identifying a variety of Pareto solutions, each offering different trade-offs, instead of just a single solution. In fact, the multi-task problem is approached from a MOOP view point [40, 30], which leverages a rich literature of algorithms including MGDA, IMTL, GradNorm, RLW, PCGrad, scalarization, and so on. We note these training algorithms iteratively optimize over the  $\mathbb{R}^d$  model parameters and can be computationally costly (in order to instantiate and modify the per-task gradient). In contrast, our algorithm is a post-training MOOP over the  $\mathbb{R}^N$  scaling coefficients, which is significantly low-compute.

Many methods have been proposed to solve MOOP and derive the Pareto optimal solutions. One may leverage the scalarization technique to transform a multi-objective problem into many single-objective ones, aiming to find one solution for each problem and approximate the Pareto front. Additionally, one can solve the Karush-Kuhn-Tucker conditions, which are easy to work with, given that  $\mathbf{c}^*$  has a closed form under our quadratic approximation. Another approach is to use evolutionary algorithms, a major branch of bio-inspired search heuristics widely applied.

In order to select an appropriate MOOP algorithm, we need to take into account the computational costs and the quality of the Pareto front. For instance, many indicator-based and selection-based methods (e.g. the hypervolume indicator [2]) have a time complexity that grows super-polynomially with the number of objectives. Indeed, for  $N \geq 3$ , the MOOP is termed as the many-objective optimization, which is significantly challenging for well-established algorithms (e.g. NSGA-II and SPEA2) and requires more advanced algorithms such as  $\epsilon$ -MOEA [14], MSOPS [21], SMS-EMOA [4], and NSGA-III [13], or the KKT approach [3].

**Task arithmetic** Task arithmetic, a method of model merging that has drawn increasing attention, applies a weighted average of models (controlled by the scaling coefficients) to obtain high performance on multiple tasks simultaneously. Several existing works have studied ways to select the scaling coefficients [22, 54, 55]: [22] simply uses equal scaling, similar to Model Soup paper, which is heuristic and sub-optimal, plus the applicability is limited to certain tasks and small scales; [55] aims to learn the optimal scaling weights by using the Shannon entropy as a surrogate objective function to the cross entropy loss. However, it requires the use of unlabeled test data from all tasks. In most real-world applications, data cannot be directly shared, which is what makes model merging appealing initially [31]. In addition, such an approach only works for classification tasks due to the use of cross-entropy loss.

[51] proposed “WiSE-FIT” to perform robust fine-tuning by computing the weighted average of the pre-trained model parameters with the parameters of the models fine-tuned on different tasks, with different weights determining different trade-offs between pre-training and fine-tuning task performance. Task Arithmetic [22] adds the weighted sum of the differences between the fine-tuned model and the pre-trained model to the weights of the pre-trained model. Again, the weights are used to distinguish the importance of various models.

**Second-order Taylor expansion** In deep learning, the second-order Taylor expansion and thus the quadratic approximation on the evaluation metric is an important technique, that characterizes the metric landscape. For example, the Newton-Ralphson method is derived from it:  $\mathbf{w}_t - \mathbf{w}_{t+1} = \mathbf{H}^{-1} \mathbf{G} = \operatorname{argmin}_{\mathbf{v}} M(\mathbf{w}_t - \mathbf{v})$  given that  $M(\mathbf{w}_t - \mathbf{v}) = M(\mathbf{w}_t) - \mathbf{v} \mathbf{G} + \frac{1}{2} \mathbf{v}^\top \mathbf{H} \mathbf{v}$ . The quadratic approximation is also combined with Lipschitz smoothness ( $L$ ) in the classic convergence analysis of SGD [7, 17], through  $M(\mathbf{w}_t - \eta \mathbf{G}) \leq M(\mathbf{w}_t) - \eta \|\mathbf{G}\|^2 + \frac{L\eta^2}{2} \|\mathbf{G}\|^2$ . Interestingly, although the approximation is only accurate in the local neighborhood, it can be used to indicate the global convergence over the iterations. One reason is that state-of-the-art neural networks are usually over-parameterized and go through lazy training, meaning that the converging parameters are close to the initialization [9, 16, 1], and thus the local approximation informs on the global convergence behavior. In particular, this approximation has played important roles in the scaling laws of neural networks (e.g. Equation 3.3 in [42]), that predict the performance and select the hyperparameters before the training actually takes place.

**Federated/Private Learning** Because the model merging is a post-training approach, it can be naturally used in federated learning, which protects both the model privacy and data privacy. To be specific, for the data privacy, the only operation that requires the data is line 6 in Algorithm 1, where each dataset can be kept at one site without sharing with other sites: the  $i$ -th site holding its own data will take in the model  $\theta(\mathbf{c})$  and only share  $M_n(\theta(\mathbf{c})) \in \mathbb{R}$ ; for the model privacy, the only operator that requires an aggregation is line 5 in Algorithm 1, where each model can be kept at one site and the aggregation is privacy-preserving using a safe center site, or the secure multi-party computation without a center site.

**Multi-Task Learning** Multi-task learning (MTL) algorithms are designed to enhance the performance of several related tasks by learning them concurrently. These algorithms typically build a shared parameter representation to integrate multiple tasks. Although, the primary emphasis of most MTL algorithms is on developing shared representations, with less attention given to balancing the

trade-offs between different tasks. Existing multitask learning strategies achieve this by computing a set of Pareto optimal solutions [30, 40, 24], yet they still require extensive and expensive training.

**Bayesian Optimization** Bayesian optimization has been widely used in scenarios that require efficient exploration of parameter spaces, particularly when evaluating the performance of each configuration is costly or time-consuming. This method is especially advantageous in machine learning and hyperparameter tuning, where traditional optimization techniques may be computationally prohibitive. Popular Bayesian optimization methods and applications are [48, 23, 33, 37, 43].

## B Nested merging scheme

Table 5: Computational cost of model merging for  $N$  models.

	# evals per task	minimum # evals (total)	# evals (total)
Naive model merging	$O(N^2)$	$O(N^3)$	$O(N \cdot 2^N)$
Nested model merging	$O(1)$	$O(N \log_2^N)$	$O(N \log_2^N)$

To estimate the computational complexity, we  $N/2 \times 2 + \dots + N/2^m \times 2^m = O(N \log_2^N)$  where  $2^{m-1} < N \leq 2^m$ .

In our experiments, we explored the strategy of decomposing tasks into pairs, identifying the Pareto front for each pair, and then sequentially merging these binary-combined models two at a time. Our goal was to determine if this incremental merging approach affects performance negatively when compared to merging multiple models in a single operation.

The results are summarized in the table below, which compares the outcomes of merging four models using both the nested merging approach and the direct merging approach. In the nested merging method, we initially merged the pairs SUN397 with DTD and GTSRB with Cars to form two combined models. Each objective metric was weighted equally at 0.5, and the optimal combinations were selected from the Pareto fronts to create the two preliminary merged models. These were subsequently merged into a final model. In contrast, the direct merging approach combines all four models simultaneously.

Contrary to our expectations, the performance of the nested merging approach was comparable to that of merging all four models at once. However, a potential disadvantage of the nested approach is that it does not allow the practitioners to explore the Pareto front as thoroughly as the direct merging method. Nevertheless, the nested merging strategy could be advantageous for practitioners who prefer to work with a predefined weighting scheme for different objectives.

We also want to mention that, in the Algorithm 2, for simplicity of illustration, we use a preference weight as an example of preference representation. However, preference can be complex and interdependent on multiple tasks. In these complex scenarios, the number of tasks in each cluster does not need to be two because it is necessary to group interdependent tasks within the same cluster. For example, consider a case where the total number of tasks  $N$  is four, and the user preference is specified as follows: If  $M_1 > \frac{1}{2}(M_2 + M_3)$ , then maximize  $M_1 + M_4$ . Otherwise, maximize  $\frac{1}{2}(M_2 + M_3) + M_4$ .  $M_n$  is the metric of task  $N$ . In this case, preferences of task 1, 2 and 3 are interdependent. Thus, we have to put them into the same cluster. In extreme cases, where all tasks are interdependent based on the given preferences, it is necessary to group all tasks into a single cluster. This scenario causes the nested merging algorithm to degenerate into the algorithm 1.

## C Proof: Negligibility of the Remainder in Multivariate Taylor Series

**Corollary: Accurate Local Approximation by Taylor Expansion** If  $f : \mathbb{R}^n \rightarrow \mathbb{R}$  is  $(k + 1)$  times continuously differentiable in a neighborhood around a point  $a \in \mathbb{R}^n$ , then the Taylor polynomial  $T_k(x)$  of order  $k$  provides an accurate approximation of  $f(x)$  when  $x$  is sufficiently close to  $a$ . Furthermore, the remainder term  $R_k(x)$  becomes negligibly small as  $\|x - a\|$  approaches zero, assuming that the  $(k + 1)$ th derivatives of  $f$  are bounded by a constant  $M$  in the neighborhood between  $a$  and  $x$ .

**Proof** Consider the Taylor series expansion of  $f$  around the point  $a$ , truncated at order  $k$ :

$$T_k(x) = \sum_{|\alpha| \leq k} \frac{D^\alpha f(a)}{\alpha!} (x - a)^\alpha$$

where  $\alpha$  is a multi-index of non-negative integers,  $D^\alpha f(a)$  denotes the partial derivatives of  $f$  at  $a$  corresponding to  $\alpha$ , and  $(x - a)^\alpha = (x_1 - a_1)^{\alpha_1} \cdots (x_n - a_n)^{\alpha_n}$ .

**Assumptions**

1. Proximity:  $\|x - a\| \rightarrow 0$  where  $\|\cdot\|$  denotes the Euclidean norm in  $\mathbb{R}^n$ .
2. Bounded Derivatives: There exists a constant  $M$  such that for all multi-indices  $\alpha$  with  $|\alpha| \equiv k + 1$ , the norm of the tensor  $D^\alpha f$  evaluated at any point  $\xi$  between  $a$  and  $x$  is bounded by  $M$ .

$$\|D^\alpha f(\xi)\| = \sup_{\|v_1\|=1, \dots, \|v_{k+1}\|=1} |D^\alpha f(\xi)(v_1, \dots, v_{k+1})| \leq M$$

The remainder term of the Taylor series expansion is given by:

$$R_k(x) = \sum_{|\alpha|=k+1} \frac{D^\alpha f(\xi)}{\alpha!} (x - a)^\alpha$$

Given the assumptions, we estimate:

$$|R_k(x)| \leq \sum_{|\alpha|=k+1} \frac{\|D^\alpha f(\xi)\|}{\alpha!} \|x - a\|^{k+1} \leq \sum_{|\alpha|=k+1} \frac{M}{\alpha!} \|x - a\|^{k+1}$$

As  $\|x - a\| \rightarrow 0$ , the term  $\|x - a\|^{k+1}$  goes to zero. Thus, the remainder term  $R_k(x)$  becomes arbitrarily small, making it negligible.

In conclusion, under the stated assumptions, the Taylor series truncated at order  $k$ ,  $T_k(x)$ , provides an accurate approximation of  $f(x)$  near  $a$ , and the remainder  $R_k(x)$  can be ignored as  $\|x - a\| \rightarrow 0$  and the higher-order derivatives remain bounded by  $M$ .



## D Additional Experiment Results

### D.1 Zero-shot Medical Image Classification

In addition to natural images, we used another dataset consisting of over 112,000 chest X-rays and 30,000 unique patients [36]. It originally contained 15 classes (14 diseases and 1 class for no finding). We split the dataset into two groups, where medical task 1 specifically tries to classify Atelectasis, Consolidation, Infiltration, Pneumothorax, and medical task 2 tries to classify Nodule, Mass and Hernia. An example image taken from the dataset is shown in Figure 6 (a).

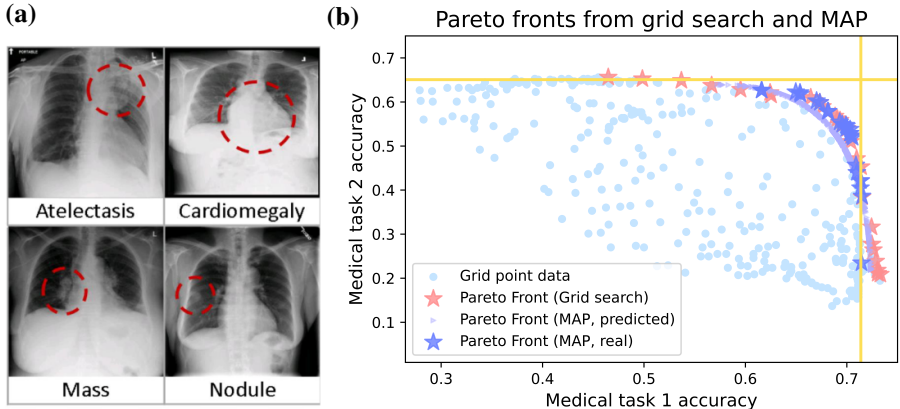


Figure 6: (a) Example figure from the NIH [36] dataset. (b) Pareto fronts found by brute-force direct search using 400 points and by MAP using 30 points. We randomly sampled 25 points from the predicted Pareto front by MAP. The resulting IGD is 0.016, and GD is 0.014.

### D.2 Merging language model

We merged French and Arabic, as well as Chinese and Japanese. Please refer to Table 6 and Appendix D.2. As we can see, the ground truth Pareto front is not in good shape. There are only a few points on the ground truth Pareto fronts which means few merged models could dominate the rest and the trade-off between the metrics of different languages might not be very significant. Even under this condition, our algorithm is still able to find out the Pareto fronts. We further try to merge ‘Arabic+French’ and ‘Chinese+Japanese’ in the nested scheme, Algorithm 2 with various preferences. However, the Pareto front usually only contains a single model which prevents us from predicting a Pareto front.

Table 6: Llama-3 fine-tuned models merging

	GD	IGD	GD+IGD
Arabic+French	0.023 <sub>0.010</sub>	0.035 <sub>0.018</sub>	0.058 <sub>0.028</sub>
Chinese+Japanese	0.014 <sub>0.013</sub>	0.028 <sub>0.017</sub>	0.041 <sub>0.026</sub>

### D.3 Bayesian adaptive sampling experiments detail

Please refer to Table 7 as the detailed experiments result for Bayesian adaptive sampling. The very left column shows the name of the 2 tasks being merged. Below, we define points (pts) as scaling coefficients and evaluation metrics of the corresponding merged models.

All of these experiments are initialized with 6 pairs of  $\mathbf{c}$ ,  $\{M_n\}_{n=1}^N$  (iter 0). In every following iteration, we sample more points following the Bayesian adaptive sampling algorithm. We compare the Bayesian adaptive sampling beginning with 6 points and adding 3 additional points (6+3 pts) with running Algorithm 1 with 9 points in a row. We also compare the Bayesian adaptive sampling beginning with 6 points and adding 3 additional points for 2 times (6+2 × 3 pts) with running Algorithm 1 with 12 points in a row. We show that, under most cases, utilizing the same number of points, Bayesian adaptive sampling performs better than the run-in-a-row scheme in Algorithm 1.

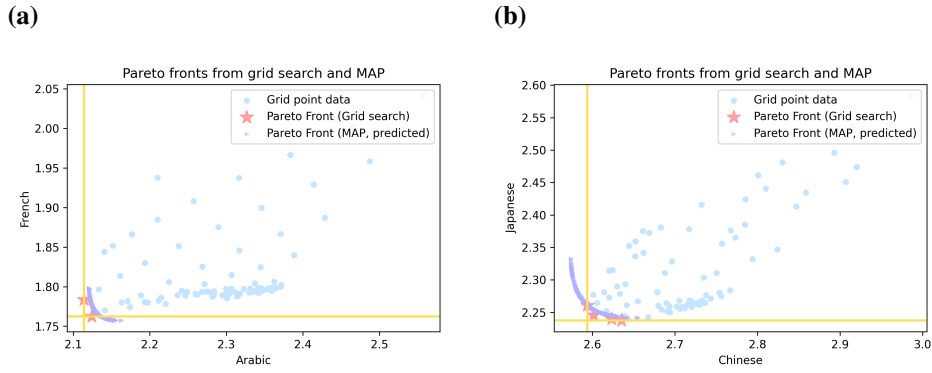


Figure 7: (a) Amortized Pareto front on merging Llama-3 fine-tuned on French with Llama-3 fine-tuned on Arabic; (b) Amortized Pareto front on merging Llama-3 fine-tuned on Chinese with Llama-3 fine-tuned on Japanese

Table 7: Detailed experiments using Bayesian adaptive sampling. In ‘Iter 0, 6 pts’, the method starts with an initial set of 6 points. In ‘Iter 1, 6+3 pts’, the method begins with 6 points and adds 3 additional points based on the Bayesian adaptive sampling results from the previous iteration. ‘Iter 2, 6+3 pts’ follows the same procedure as ‘Iter 1, 6+3 pts’. In ‘Init  $n$ ’, the experiment runs the Algorithm 1 with  $n$  points in a row.

	GD	IGD	GD+IGD	$R_1^2$	$R_2^2$
DTD+Cars (Iter 0, 6 pts)	0.265 <sub>0.16</sub>	0.213 <sub>0.161</sub>	0.478 <sub>0.251</sub>	-2.708 <sub>4.513</sub>	-1.774 <sub>2.791</sub>
DTD+Cars (Iter 1, 6+3 pts)	0.195 <sub>0.133</sub>	0.109 <sub>0.172</sub>	0.303 <sub>0.273</sub>	-1.475 <sub>3.769</sub>	0.576 <sub>0.73</sub>
DTD+Cars (Iter 2, 6+2*3 pts)	0.1 <sub>0.076</sub>	0.018 <sub>0.008</sub>	0.118 <sub>0.075</sub>	0.489 <sub>0.647</sub>	0.902 <sub>0.113</sub>
DTD+Cars (Init 9)	0.086 <sub>0.085</sub>	0.024 <sub>0.014</sub>	0.11 <sub>0.085</sub>	0.606 <sub>0.497</sub>	0.85 <sub>0.144</sub>
DTD+Cars (Init 12)	0.099 <sub>0.117</sub>	0.034 <sub>0.025</sub>	0.132 <sub>0.113</sub>	0.742 <sub>0.148</sub>	0.922 <sub>0.078</sub>
DTD+RESISC45 (Iter 0, 6 pts)	0.178 <sub>0.054</sub>	0.111 <sub>0.129</sub>	0.289 <sub>0.175</sub>	-2.677 <sub>5.195</sub>	0.359 <sub>0.694</sub>
DTD+RESISC45 (Iter 1, 6+3 pts)	0.067 <sub>0.062</sub>	0.051 <sub>0.027</sub>	0.118 <sub>0.059</sub>	0.715 <sub>0.2</sub>	0.003 <sub>0.717</sub>
DTD+RESISC45 (Iter 2, 6+2*3 pts)	0.049 <sub>0.05</sub>	0.052 <sub>0.035</sub>	0.101 <sub>0.049</sub>	0.813 <sub>0.088</sub>	0 <sub>0.74</sub>
DTD+RESISC45 (9)	0.092 <sub>0.084</sub>	0.018 <sub>0.008</sub>	0.11 <sub>0.089</sub>	0.7 <sub>0.389</sub>	0.351 <sub>1.101</sub>
DTD+RESISC45 (Init 12)	0.056 <sub>0.048</sub>	0.026 <sub>0.013</sub>	0.082 <sub>0.039</sub>	0.796 <sub>0.079</sub>	0.801 <sub>0.222</sub>
EuroSAT+RESISC45 (Iter 0, 6 pts)	0.279 <sub>0.137</sub>	0.061 <sub>0.047</sub>	0.341 <sub>0.178</sub>	-4.381 <sub>4.102</sub>	-1.028 <sub>1.668</sub>
EuroSAT+RESISC45 (Iter 1, 6+3 pts)	0.154 <sub>0.069</sub>	0.019 <sub>0.012</sub>	0.173 <sub>0.066</sub>	-1.888 <sub>2.977</sub>	0.557 <sub>0.224</sub>
EuroSAT+RESISC45 (Iter 2, 6+2*3 pts)	0.148 <sub>0.051</sub>	0.056 <sub>0.076</sub>	0.204 <sub>0.077</sub>	-1.085 <sub>0.896</sub>	0.513 <sub>0.215</sub>
EuroSAT+RESISC45 (Init 9)	0.147 <sub>0.084</sub>	0.075 <sub>0.092</sub>	0.222 <sub>0.134</sub>	-1.419 <sub>2.475</sub>	0.213 <sub>0.75</sub>
EuroSAT+RESISC45 (Init 12)	0.182 <sub>0.099</sub>	0.059 <sub>0.076</sub>	0.242 <sub>0.166</sub>	-0.722 <sub>1.182</sub>	0.724 <sub>0.275</sub>
GTSRB+Cars (Iter 0, 6 pts)	0.394 <sub>0.128</sub>	0.203 <sub>0.083</sub>	0.597 <sub>0.122</sub>	-1.549 <sub>3.747</sub>	-1.089 <sub>0.58</sub>
GTSRB+Cars (Iter 1, 6+3 pts)	0.085 <sub>0.062</sub>	0.025 <sub>0.018</sub>	0.11 <sub>0.074</sub>	-0.28 <sub>1.745</sub>	0.937 <sub>0.087</sub>
GTSRB+Cars (Iter 2, 6+2*3 pts)	0.036 <sub>0.011</sub>	0.02 <sub>0.021</sub>	0.055 <sub>0.018</sub>	0.617 <sub>0.268</sub>	0.962 <sub>0.037</sub>
GTSRB+Cars (Init 9)	0.205 <sub>0.118</sub>	0.186 <sub>0.152</sub>	0.391 <sub>0.244</sub>	-1.111 <sub>1.992</sub>	-0.529 <sub>1.742</sub>
GTSRB+Cars (Init 12)	0.091 <sub>0.044</sub>	0.046 <sub>0.052</sub>	0.138 <sub>0.082</sub>	-0.177 <sub>1.533</sub>	0.93 <sub>0.046</sub>
GTSRB+RESISC45 (Iter 0, 6 pts)	0.13 <sub>0.092</sub>	0.111 <sub>0.066</sub>	0.241 <sub>0.076</sub>	-2.81 <sub>1.772</sub>	-1.037 <sub>1.184</sub>
GTSRB+RESISC45 (Iter 1, 6+3 pts)	0.059 <sub>0.007</sub>	0.04 <sub>0.067</sub>	0.098 <sub>0.067</sub>	0.449 <sub>0.493</sub>	0.615 <sub>0.363</sub>
GTSRB+RESISC45 (Iter 2, 6+2*3 pts)	0.038 <sub>0.011</sub>	0.043 <sub>0.065</sub>	0.081 <sub>0.074</sub>	0.672 <sub>0.171</sub>	0.642 <sub>0.313</sub>
GTSRB+RESISC45 (Init 9)	0.075 <sub>0.056</sub>	0.056 <sub>0.07</sub>	0.131 <sub>0.085</sub>	-0.676 <sub>2.08</sub>	0.76 <sub>0.364</sub>
GTSRB+RESISC45 (Init 12)	0.105 <sub>0.052</sub>	0.017 <sub>0.013</sub>	0.122 <sub>0.061</sub>	0.721 <sub>0.39</sub>	0.863 <sub>0.169</sub>
RESISC45+SVHN (Iter 0, 6 pts)	0.168 <sub>0.161</sub>	0.09 <sub>0.092</sub>	0.258 <sub>0.15</sub>	-1.005 <sub>2.14</sub>	-1.415 <sub>2.14</sub>
RESISC45+SVHN (Iter 1, 6+3 pts)	0.12 <sub>0.043</sub>	0.058 <sub>0.075</sub>	0.179 <sub>0.069</sub>	0.822 <sub>0.156</sub>	0.12 <sub>1.539</sub>
RESISC45+SVHN (Iter 2, 6+2*3 pts)	0.099 <sub>0.038</sub>	0.058 <sub>0.076</sub>	0.157 <sub>0.081</sub>	0.749 <sub>0.249</sub>	0.206 <sub>1.482</sub>
RESISC45+SVHN (Init 9)	0.108 <sub>0.109</sub>	0.081 <sub>0.081</sub>	0.19 <sub>0.159</sub>	0.324 <sub>0.843</sub>	0.156 <sub>0.932</sub>
RESISC45+SVHN (Init 12)	0.023 <sub>0.015</sub>	0.033 <sub>0.025</sub>	0.055 <sub>0.025</sub>	0.797 <sub>0.216</sub>	0.782 <sub>0.405</sub>
SUN397+SVHN (Iter 0, 6 pts)	0.221 <sub>0.144</sub>	0.075 <sub>0.108</sub>	0.296 <sub>0.195</sub>	-0.528 <sub>2.117</sub>	-2.319 <sub>3.904</sub>
SUN397+SVHN (Iter 1, 6+3 pts)	0.094 <sub>0.064</sub>	0.028 <sub>0.018</sub>	0.122 <sub>0.067</sub>	0.939 <sub>0.047</sub>	-0.412 <sub>1.255</sub>
SUN397+SVHN (Iter 2, 6+2*3 pts)	0.086 <sub>0.064</sub>	0.022 <sub>0.005</sub>	0.108 <sub>0.066</sub>	0.954 <sub>0.029</sub>	-0.228 <sub>0.925</sub>
SUN397+SVHN (Init 9)	0.112 <sub>0.17</sub>	0.031 <sub>0.014</sub>	0.143 <sub>0.181</sub>	0.216 <sub>1.643</sub>	-0.647 <sub>2.573</sub>
SUN397+SVHN (Init 12)	0.083 <sub>0.088</sub>	0.024 <sub>0.005</sub>	0.107 <sub>0.085</sub>	0.922 <sub>0.046</sub>	0.639 <sub>0.453</sub>

## D.4 Additional experiment results on ResNet

We performed additional experiments on ResNet18 [18] on CIFAR10 [28] and Flowers102 [35] and show the Pareto front obtained in Figure 8. Unlike ViT models which perform zero-shot classification, ResNet requires additional fine-tuning of the classification head after model merging. We demonstrate that our method still applies to those models.

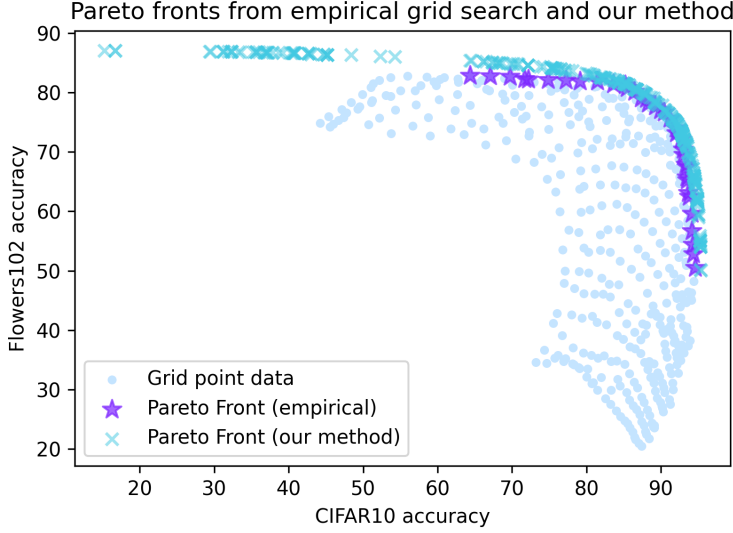


Figure 8: Pareto front obtained for two ResNet18 models on CIFAR10 and Flowers 102. We perform additional finetuning of the classification head after merging the model weights.

## E More details about algorithms

### E.1 Algorithm 1

In this section, we extend the discussion on line 7 of the algorithm and on Remark 1. In (6), the optimization problem is essentially minimizing the mean squared error (MSE) of a linear regression. The predictors are  $\mathbf{C} = \text{concat}(c_1^2, c_2^2, \dots, c_T^2, c_1 c_2, c_1 c_3, \dots, c_{T-1} c_T, c_1, c_2, \dots, c_T, 1)$ , the variables are  $(\mathbf{A}_n^*, \mathbf{b}_n^*, e_n^*)$ , and the responses are  $M_n(\boldsymbol{\theta}_m(\mathbf{c}))$ . Subscripts denote standard deviations over 6 runs.

We can certainly seek other designs to improve the accuracy and robustness of  $(\mathbf{A}_n^*, \mathbf{b}_n^*, e_n^*)$ . On one hand, we can use other loss functions like mean absolute error or Huber loss, while still using the linear regression. On the other, we can modify  $\tilde{M}_n(\mathbf{c})$ . If the metric  $M_n$  has a specific bounded region, we could restrict the fitting interval. For example, if the metric is the accuracy or F1 score between 0 and 1, we could switch the definition to  $\tilde{M}_n(\mathbf{c}; \mathbf{A}_n, \mathbf{b}_n, e_n) \equiv \text{sigmoid}(e_n + \mathbf{b}_n^\top \mathbf{c} + \frac{1}{2} \mathbf{c}^\top \mathbf{A}_n \mathbf{c})$ . This is equivalent to a logistic regression with the same definition of predictors and responses as the linear regression. If the metric is loss, which ranges from 0 to positive infinity, then we could switch to  $\tilde{M}_n(\mathbf{c}; \mathbf{A}_n, \mathbf{b}_n, e_n) \equiv \text{softplus}(e_n + \mathbf{b}_n^\top \mathbf{c} + \frac{1}{2} \mathbf{c}^\top \mathbf{A}_n \mathbf{c})$ . In summary, one may extend (6) to

$$\mathbf{A}_n^*, \mathbf{b}_n^*, e_n^* = \arg \min_{\mathbf{A}_n, \mathbf{b}_n, e_n} \text{MSE} \left( M_n(\boldsymbol{\theta}_{\text{merge}}(\mathbf{c})), \sigma(\tilde{M}_n(\mathbf{c}; \mathbf{A}_n, \mathbf{b}_n, e_n)) \right),$$

and replace MSE and  $\sigma = \mathbb{I}$  with other functions.

We emphasize that Algorithm 1 is an out-of-box plugin-like method. Many parts of it are kept generic: there are multiple ways to sample  $\Omega$  in terms of the number of  $\mathbf{c}$  and the style of sampling (Bayesian or not), thus creating a tradeoff between the quality of Pareto front and the computational time; the task vector can be computed on the more memory-capable CPU and possibly in a parameter-efficient manner (e.g. LoRA, Adapter, and BiTFiT): for example, computing  $\mathbf{v}_n$  via the subtraction of two full 7B models requires  $2 \times 23 = 46\text{GB}$  of memory capacity, but the memory cost for PEFT models

may reduce to 16MB by only subtracting the non-frozen components; the for-loops in line 2 and 4 can be computed in parallel, possibly using a much smaller subset of the data, and thus enjoying a computational speed-up.

**Remark 1 (quadratic surrogate model fitting)** In Algorithm 1,  $\mathbf{A}_n^*$ ,  $\mathbf{b}_n^*$ ,  $c_n^*$  in (6) can be readily solved by off-the-shelf methods, such as close-form solution (if applicable), LBFGS, Newton’s method and gradient descent, since this is a convex problem. In Appendix E, we generalize the ways to learn the coefficients in (5), besides minimizing the mean square error in (6).

### E.2 Algorithm 2

In this section, we explain the operations of the algorithm in Figure 3 in details. Here task 1 to 8 is Cars, GTSRB, DTD, SUN397, Resisc45, and SVHN. If we minimize (4) without the nested merging, we would need to estimate  $\mathbf{A}_1, \dots, \mathbf{A}_8 \in \mathbb{R}^{8 \times 8}$ , with hundreds of  $\mathbf{c}$ .

With the nested merging, for the first round, we merge  $(\theta_{ft}^1, \theta_{ft}^2)$  into  $\theta_{merge}^{1,2}$ , thus approximating  $\mathbf{A}_1$  and  $\mathbf{A}_2 \in \mathbb{R}^{8 \times 8}$  by  $\mathbf{A}_1[1 : 2, 1 : 2]$  and  $\mathbf{A}_2[1 : 2, 1 : 2] \in \mathbb{R}^{2 \times 2}$ , respectively. That is, we only care about the interference between task 1 and 2, but not task 1 and 5. Similarly, we merge  $(\theta_{ft}^3, \theta_{ft}^4)$  into  $\theta_{merge}^{3,4}$ , and  $(\theta_{ft}^5, \theta_{ft}^6)$  into  $\theta_{merge}^{5,6}$ . Next, we merge  $(\theta_{merge}^{1,2}, \theta_{merge}^{3,4})$  into  $\theta_{merge}^{1,2,3,4}$ , and finally into  $\theta_{merge}^{1,2,3,4,5,6,7,8}$ .

### E.3 Algorithm 3

Algorithm 4 is a detailed version of Algorithm 3. Figure 9 includes an illustration of our discretization method (how we create bins) in 2D and 3D decision variable ( $\mathbf{c}$ ) space.

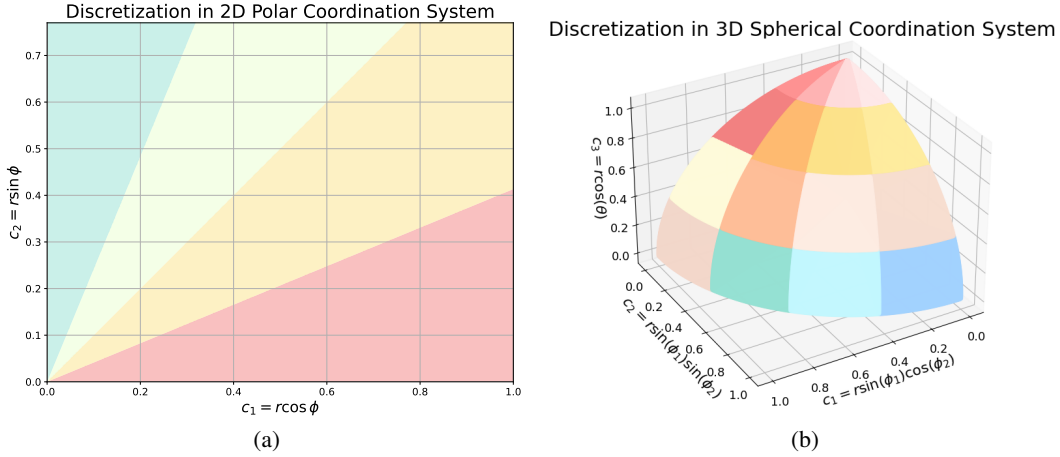


Figure 9: (a) Discretizing of two task scaling coefficients along the angular dimension in 2D polar coordinate system; (b) Discretizing of three task scaling coefficients along the angular dimensions in 3D spherical coordinate system;

---

**Algorithm 4** Bayesian Adaptive of Surrogate Model

---

**Require:** Number of iterations  $J$ , Buffer  $\mathcal{B}$ , Pretrained model  $\theta_{\text{pre}}$ , Task vectors  $\mathbf{v}_n$ , Evaluators for task  $N$ ,  $M_n(\cdot)$ , Discretization bin number  $K$ , sample size for every iteration  $n_j$ ,  $j = 0$  to  $J$ , Bootstrap dropping rate  $\alpha = 20\%$ , Bootstrap sampling number  $Q = 30$ .

- 1:  $\mathcal{B} \leftarrow \emptyset$
  - 2: **for**  $j = 0$  to  $J$  **do**
  - 3:   **if**  $j = 0$  **then**
  - 4:     Sample  $n_0$  scaling coefficients  $\{\mathbf{c}_i\}_{i=1}^{n_j}$  from  $U([0, 1]^T)$
  - 5:   **else**
  - 6:     Sample  $n_j$  scaling coefficients  $\{\mathbf{c}_i\}_{i=1}^{n_j}$  based on the posterior distribution
  - 7:   **for**  $i = 0$  to  $n_j$  **do**
  - 8:     Merge the model  $\theta_m(\mathbf{c}_i) = \theta_{\text{pre}} + \mathbf{c}_i \cdot \mathbf{v}_n$
  - 9:     Evaluate  $m_{n,i} = M_n(\theta_m(\mathbf{c}_i))$
  - 10:     $\mathcal{B} \leftarrow \mathcal{B} \cup \{(\mathbf{c}_i, m_{n,i})\}$
  - 11:   Fit the quadratic approximation surrogate model  $\tilde{M}_n$  by learning  $\mathbf{A}_n^*$ ,  $\mathbf{b}_n^*$ ,  $e_n^*$  in (6).
  - 12:   Discretize the scaling coefficients along the angular dimensions in hyper-spherical coordinates (see figure 9 as examples)
  - 13:   **for**  $k = 0$  to  $K$  **do**
  - 14:     Calculate the mean of  $L2$  loss between  $\tilde{M}_n(\mathbf{c}_i)$  and  $M_t(\mathbf{c}_i)$ , where  $\mathbf{c}_i$  are in bin  $k$ , denoted as  $\text{mean}_k$   
   {Bootstrap to estimate the standard deviation of the losses.}
  - 15:     **for**  $q = 0$  to  $Q$  **do**
  - 16:       Randomly (uniformly) drop  $\alpha$  scaling coefficient in bin  $k$
  - 17:       Calculate the mean of  $L2$  loss between  $\tilde{M}_n(\mathbf{c}_i)$  and  $M_t(\mathbf{c}_i)$  with the rest points and denoted with  $l_q$
  - 18:       Calculate the standard deviation of the  $\{l_q\}_{q=0}^Q$  and denoted as  $\text{std}_k$
  - 19:        $\text{score}_k = \text{mean}_k + \frac{1}{2}\text{std}_k$
  - 20:     Calculate probability distribution across the discretized bins by  $\text{score}_k$  as the posterior sampling strategy in the next round
  - 21: **return**
-